Published in final edited form as:
Sci Signal. ; 7(347): ra97. doi:10.1126/scisignal.2005413.

Temporal and Spatial Regulation of Epsin Abundance and VEGFR3 Signaling are Required for Lymphatic Valve Formation and Function

Xiaolei Liu[1,2], **Satish Pasula**[1], **Hoogeun Song**[1], **Kandice L. Tessneer**[1], **Yunzhou Dong**[1], **Scott Hahn**[1], **Tadayuki Yago**[1], **Megan Brophy**[1,2], **Baojun Chang**[1], **Xiaofeng Cai**[1], **Hao Wu**[1], **John McManus**[1], **Hirotake Ichise**[3], **Constantin Georgescu**[4], **Jonathan D. Wren**[2,4], **Courtney Griffin**[1,5], **Lijun Xia**[1,2], **R. Sathish Srinivasan**[1], and **Hong Chen**[1,2,*]

[1]Cardiovascular Biology Program, Oklahoma Medical Research Foundation, Oklahoma, OK 73104, USA

[2]Department of Biochemistry and Molecular Biology, University of Oklahoma Health Science Center, Oklahoma, OK 73104, USA

[3]Laboratory of Developmental Genetics, Center for Experimental Medicine and Systems Biology, Institute of Medical Science, University of Tokyo, Minato-ku, Tokyo 108-8639, Japan

[4]Arthritis & Clinical Immunology Research Program, Oklahoma Medical Research Foundation, Oklahoma, OK 73104, USA

[5]Department of Cell Biology, University of Oklahoma Health Sciences Center, Oklahoma, OK 73126, USA

Abstract

Lymphatic valves prevent the backflow of the lymph fluid and ensure proper lymphatic drainage throughout the body. Local accumulation of lymphatic fluid in tissues, a condition called lymphedema, is common in individuals with malformed lymphatic valves. The vascular endothelial growth factor receptor 3 (VEGFR3) is required for the development of lymphatic vascular system. The abundance of VEGFR3 in collecting lymphatic trunks is high before valve formation and, except at valve regions, decreases after valve formation. We found that in mesenteric lymphatics, the abundance of epsin 1 and 2, which are ubiquitin-binding adaptor proteins involved in endocytosis, was low at early stages of development. After lymphatic valve formation, the initiation of steady shear flow was associated with an increase in the abundance of epsin 1 and 2 in collecting lymphatic trunks, but not in valve regions. Epsin 1 and 2 bound to VEGFR3 and mediated the internalization and degradation of VEGFR3, resulting in termination of VEGFR3 signaling. Mice with lymphatic endothelial cell-specific deficiency of epsin 1 and 2

*To whom correspondence should be addressed. hong-chen@omrf.org, Telephone: 405-271-2750, Fax: 405-271-3137.

AUTHOR CONTRIBUTIONS: H. C. designed the project and experiments and wrote the manuscript; X. L. wrote the manuscript and performed most of experiments; S. P., B. C., K. T., X. C., M. B., and J. M. helped with in vivo experiments; S. H., and H. I. helped with transgenic mouse models; Y. D., H. S., and H. W. helped with statistical analysis; C.G. and J. D. W. helped with statistical validation; T. Y. helped perform the shear flow experiments in vitro; C. G., L. X., and R. S. S. helped with writing the manuscript. All authors contributed and commented on the manuscript.

COMPETING INTERESTS: The authors declare that they have no competing interests.

had dilated lymphatic capillaries, abnormally high VEGFR3 abundance in collecting lymphatics, immature lymphatic valves, and defective lymph drainage. Deletion of a single *Vegfr3* allele or pharmacological suppression of VEGFR3 signaling restored normal lymphatic valve development and lymph drainage in epsin-deficient mice. Our findings establish a critical role for epsins in the temporal and spatial regulation of VEGFR3 abundance and signaling in collecting lymphatic trunks during lymphatic valve formation.

INTRODUCTION

The lymphatic vascular system plays a fundamental role in collecting extravasated fluid, macromolecules, and immune cells from tissues and returning them to the blood circulation (1). The signaling cascade that initiates lymphatic development begins with the transcription factor Sox18 in a subpopulation of cardinal vein endothelial cells. Sox18 cooperates with the transcription factor Coup-TFII (which is already present in the cardinal vein) to increase the abundance of Prox1 (2, 3, 4). Prox1 is the first marker of lymphatic endothelial cells (LECs) (4, 5). LEC precursors sprout and migrate to form a primary lymph sac that further expands to form a primary lymphatic network at E14.5 in mice (6, 7). Separation of lymphatic and blood vessels involves Podoplanin-CLEC-2-mediated signaling (8). Podoplanin in LECs is a ligand for CLEC-2, which is a c-type lectin receptor in platelets. Separation of lymphatic network from blood circulation requires signaling mediated by the tyrosine kinase SYK and SLP-76 (Src-homology 2 domain-containing leukocyte protein of 76 kDa) downstream of activation of CLEC-2 (8, 9).

The primary lymphatic network is further remodeled to form a mature lymphatic system consisting of lymphatic capillaries and collecting lymphatic vessels. Lymphatic capillaries are blind-ended vessels formed from a single layer of LECs with very permeable, button-like junctions that allow the uptake of tissue fluid (lymph). In contrast, mature collecting lymphatic vessels are surrounded by a basement membrane, pericytes, and smooth muscle cells (10). Collecting lymphatic vessels also have lymphatic valves to enhance the unidirectional flow of lymph (11). The major stages for embryonic valve formation include the initiation of lymphatic valve formation at embryonic (E) day E16 with increased abundance of Prox1 and Foxc2 (12). Mice without Foxc2 do not develop lymphatic valves and have abnormal lymph flow (13). Clusters of Prox1-positive lymphatic valve-covering LECs then form a ring-like structure that extends and matures into V-shaped leaflets that can prevent lymph backflow. Following initial valve formation, Prox1 and Foxc2 are reduced in the lymphatic trunk LECs. Lymph flow-mediated mechanical stimulus (12) and molecules such as Ephrin-B2 (14), CX37, CX43 (15), Semaphorin3a, Neuropilin 1 (16, 17), integrin-α9 (18) and bone morphogenetic protein 9 (BMP9) (19) are thought to play roles in lymphatic valve formation or maturation. Lymphatic valves are crucial for efficient lymph transport. Impairments of lymphatic development and function, potentially in conjunction with fibrosis and infection, are implicated in various progressive and life-threatening human primary lymphedema syndromes (20). Furthermore, lymph nodes and collecting lymphatic vessels are commonly embedded in adipose tissues and are important for lipid metabolism. Perinodal adipose tissue constantly undergoes dynamic inflammatory challenges, which suggests a functional link between dysfunctional lymphatic vessels and obesity-associated

metabolic diseases (21, 22). However the mechanisms of lymphatic valve morphogenesis remain elusive. Collecting lymphatic vessels form at E14.5 – E15.5, corresponding with high VEGFR3 abundance in the lymphatic trunk LECs (23). Moreover, VEGFR3 abundance in the lymphatic trunk endothelial cells decreases at E17.5, a key event in the formation of lymphatic valves (23). However, the mechanism with which VEGFR3 abundance in the collecting lymphatic vessels is temporally regulated is poorly understood. Previous studies of the distribution and function of VEGFR3 signaling have mainly focused on early lymphatic development and lymphangiogenesis in which VEGFR3 and its ligand VEGF-C are required for the survival, maintenance, and migration of endothelial cells in lymphatic vessels during early developmental periods (1, 24, 25). Understanding how VEGFR3 abundance is deceased in collecting lymphatic trunk LECs is important to decipher the development of the collecting lymphatic system.

Epsins are a family of ubiquitin-binding endocytic clathrin adaptors (26, 27, 28). Three epsin isoforms are present in mammals: epsin 1 and 2 are present in all tissues (29), whereas epsin 3 is exclusively found in the stomach (30). Mice lacking either epsin 1 or epsin 2 reach adulthood and appear normal, suggesting functional redundancy. However, mice lacking both epsin 1 and 2 die at E10, suggesting that these epsins have essential developmental functions (29). To study the role of epsins in the vascular endothelium, we have previously generated endothelial cell-specific epsin 1 and 2 knockout mice (EC-DKO). We have shown that endothelial cell-specific or post-developmental inducible deletion of epsin 1 and 2 in adult mice reduces tumor angiogenesis by selectively impairing internalization of VEGFR2 and enhancing VEGF signaling in tumor vasculature (31).

In this study, we used lymphatic endothelial cell type-specific constitutive and inducible mouse genetics to investigate the roles of epsins in lymphatic development and VEGFR3 regulation.

RESULTS

Loss of epsins impaired collecting lymphatic valve formation in mice at embryonic and early postnatal stages

To explore the roles of epsins in lymphatic development and function, we selectively ablated epsin 1 and 2 in LECs by crossing *epsin 1*$^{fl/fl}$; *epsin 2*$^{-/-}$ mice (29, 31), with *LYVE-1*-Cre or *Prox1-CreER*^{T2} mice which express Cre recombinase specifically in LECs to generate lymphatic-specific epsin-deficient mice (LEC-DKO) or tamoxifen-inducible lymphatic-specific epsin-deficient mice (LEC-iDKO), respectively (Fig. S1A, B). Mouse LECs were isolated and purified from the mesenteries of wild-type or epsin-deficient mice with anti-podoplanin beads. Purified LECs were characterized with immunostaining against LYVE-1; approximately 90% of the purified cells were LYVE-1 positive LECs (Fig. S1C). The purity of LECs was further confirmed by flow cytometry using antibody against VEGFR3 (Fig. S1D). Deletion of epsin 1 and 2 in LECs purified from LEC-DKO and LEC-iDKO were validated by Western blotting and qRT-PCR analysis (Fig. S1E–H).

Because LEC-DKO and LEC-iDKO mice were viable and appeared normal, we examined the collecting lymphatic vessels and lymphatic valves in these mice at different

developmental stages. Development of mesenteric collecting lymphatic vessels begins at E14.5 – E15.5, when a mesh-like network of lymphatic vessels is formed by LECs surrounding the mesenteric arteries and veins (23). Whole mount staining revealed similar mesh-like networks of mesenteric collecting lymphatic vessels with capillary like structures along and across the blood vessels in both wild-type and LEC-DKO E15.5 embryos (Fig. S2A, B). The morphology of collecting lymphatic vessels changed substantially at E16.5 such that the collecting lymphatic vessels started to fuse to form big lymphatic trunk with few branches (Fig. S2C, D). By E17, lymphatic trunks were well formed (Fig. S2E, F). We observed similar patterning of the collecting lymphatics in both genotypes; that is, the development of collecting lymphatic vessels was indistinguishable in both wild-type and LEC-DKO embryos from E15.5 to E17 (Fig. S2), suggesting that epsin-deficiency did not initially interfere with the collecting lymphatic vessel development. We also examined embryonic skin capillaries in wild-type and LEC-DKO embryos at E16.5 and E18.5 by whole mount staining with antibodies against VEGFR3, Prox1 and the type I transmembrane receptor Neuropillin-2, which is restricted to the vascular cell membrane in veins and lymphatic vessels (34). At E16.5, vessel diameters in both genotypes were not statistically significant (Fig. S3A–B, I). By E18.5, the lymphatic capillaries in LEC-DKO embryos were enlarged compared to those in wild-type littermates (Fig. S3C–D, I). We also examined postnatal lymphatic capillaries in wild-type and epsin-deficient pups, and found that at P0, skin and intestinal tissues from both LEC-iDKO and LEC-DKO pups had enlarged lymphatic capillaries (Fig. S4). Although the morphology of the collecting lymphatics in LEC-DKO embryos was normal at E17 (Fig. S2), these pups developed enlarged collecting lymphatic vessels at E18.5 (Fig. 1, fig. S3I), when lymphatic valves have matured (23). At E18.5, we found that the mesenteric collecting lymphatic luminal valves were well established in wild-type embryos and had two V-shaped leaflets (Fig. 1A, B). In contrast, the LEC-DKO embryos had dilated lymphatic vessels and defective valves, although Prox1 was highly abundant in the putative valve region (Fig. 1C, D). Notably, the mesenteric arteries and veins developed normally in both wild-type and LEC-DKO embryos (Fig. 1A, C). Similar to LEC-DKO embryos, LEC-iDKO embryos also had defective valve formation at E18.5 (Fig. S5A, B).

We further examined the lymphatic valve morphology at postnatal stages. Lymphatic valve morphogenesis in postnatal mice requires the interaction of integrin-α9, a marker for lymphatic leaflet formation, with its ligand, fibronectin-EIIIA FN-EIIIA in the extracellular matrix (18). At postnatal day 6 (P6), wild-type pups had mature lymphatic valves that were enriched for integrin-α9 and Prox1 in the valve region (Fig. 1E, F). In contrast, despite high Prox1 and integrin-α9 abundance in the putative valve region, LEC-DKO pups displayed mainly ring-shaped structures in the valve region with enlarged lymphatic trunks (Fig. 1G, H). At P13, LEC-DKO pups exhibited dilated collecting lymphatic trunks with malformed lymphatic valves compared to wild-type pups (Fig. 1I, J). Bright field imaging revealed chyle-filled lymphatic vessels and V-shaped luminal valves in P13 wild-type pups (Fig. 1K, L) and enlarged lymphatic trunks with ring-shaped luminal valves in LEC-DKO pups (Fig. 1M, N). Similar to LEC-DKO pups, LEC-iDKO pups at P6 also had enlarged collecting lymphatic vessels and defective leaflets in the mesenteric lymphatic valves (Fig. S5C, D). Quantification of V-shaped valves in mesenteric lymphatic vessels showed that lymphatic

valve formation was complete by E18.5 in wild-type embryos but was significantly delayed in both LEC-DKO and LEC-iDKO embryos; only 25% and 30% of the normal number of valves formed by P6 in LEC-DKO pups (Fig. 1O) and LEC-iDKO pups (Fig. S5E). These results indicated that deletion of epsin 1 and 2 in LECs results in valve maturation defects during the embryonic and early postnatal stages. We concluded that lymphatic endothelial epsin 1 and 2 are required for normal collecting lymphatic valve formation during embryonic and early postnatal development.

Loss of lymphatic endothelial epsins caused defective lymphatic drainage

Abnormal development of the lymphatic system during early embryonic stages causes edema due to failure to separate the lymphatic-venous systems, impaired lymphangiogenesis or impaired lymphovenous valve formation (5, 7, 32, 33). Loss of lymphatic endothelial epsins did not result in embryonic lethality or edema. Furthermore, although espin deficiency in LECs impaired valve formation in collecting lymphatics, our examination of LEC-DKO E17.5 embryos by immunostaining revealed normal lymph sac formation and lymphovenous valve development (Fig. S6). This suggested that epsins are not crucial for early embryonic lymphatic development and lymphovenous valve development.

To determine whether loss of epsins in lymphatic endothelial cells affects functional lymphatic drainage postnatally, we examined lymphatic transport by intradermal injection of FITC-Dextran into mouse ears. In P14 wild-type mice, FITC-Dextran was efficiently collected in a typical lymphatic drainage pattern by collecting lymphatic vessels in the ear dermis (Fig. 2A). In the ear dermis of P14 LEC-DKO mice, FITC-Dextran-filled lymphatic vessels were dilated and discontinuous (Fig. 2B). Moreover, this impaired drainage of the mutant lymphatics resulted in prominent residual FITC-Dextran staining in the surrounding tissue (Fig. 2B). As an additional means of examining lymphatic drainage, we used microlymphangiography to visualize the transport of FITC-Dextran injected intradermally into the tip of the tail. In P14 wild-type mice, FITC-Dextran was easily detectable throughout the entire tail at 8 minutes post injection (Fig. 2C). In contrast, LEC-DKO mice exhibited a blockage in FITC-Dextran transport even at 20 minutes post injection, consistent with the dysfunctional drainage seen in the ear (Fig. 2C). We also assessed popliteal lymph node drainage by injecting Evans blue dye into the hind footpads of P6 pups. The blue dye was collected by collecting lymphatic vessels into the popliteal lymph node of wild-type pups but not of LEC-DKO pups 15 min after injection (Fig. 2D), further suggesting that epsins in lymphatic endothelial cells are critical for the proper function of collecting lymphatics. Together, our results showed that lymphatic drainage in the LEC-DKO mice is severely impaired during early postnatal stages.

Steady lymph flow induced expression of epsin-encoding genes

We next investigated the expression of the genes encoding epsin 1 and 2 in LECs during development. qRT-PCR analysis of freshly isolated mesenteric LECs revealed the abundance of *epsin 1* and *epsin 2* was reduced before valve formation (at E14). *Epsin 1* and *epsin 2* gene expression was induced at E18 and sustained postnatally (Fig. 3A). Whole mount staining of collecting lymphatic vessel showed that the abundance of epsin 1 and 2 was high in lymphatic trunk LECs, which had low Prox1 abundance, but was low in valve-

covering LECs, which had high Prox1 abundance (Fig. S7, A to D). This result suggested the abundance of epsin 1 and 2 was selectively increased in lymphatic trunk LECs during valve formation (Fig. S7E). We further explored the molecular mechanisms underlying the preferential increase in epsin abundance in lymphatic trunk LECs. After their formation, collecting lymphatic vessels transport lymph and in response to this lymph flow, LECs undergo morphological and transcriptional changes (34, 35). LECs localized to areas of disturbed flow form valves while the remaining LECs elongate and align under steady flow to form lymphatic trunks (12). To test whether *epsin 1* and *2* gene expression were spatially regulated by the two types of lymph flow forces, we performed an *in vitro* laminar shear stress assay to mimic lymph flow in collecting lymphatic vessels (11). Compared to static conditions, the mRNA and protein abundance for both epsin 1 and epsin 2 were induced by laminar shear stress (Fig. 3B, Fig. S8A, B). Because shear flow activates the activity of the tyrosine kinase Src in endothelial cells (37), we also examined whether Src activity plays role in flow-induced epsin expression. qRT-PCR analysis showed shear flow-induced epsin increases were ablated by administration of the Src family kinase inhibitor PP2 (Fig. 3B), suggesting that Src kinase activity is involved in laminar shear flow-induced *epsin* expression in mouse LECs. As a positive control, we also examined the expression of *connexin 37* (*CX37*) under laminar shear stress. Consistent with previously published work (12), *CX37* expression was induced by laminar shear stress (Fig. 3B). We used an *in vitro* oscillatory shear stress assay to mimic disturbed lymph flow in collecting lymphatic valve regions (11, 12). Quantitative RT-PCR analysis showed that oscillatory fluid shear stress induced the mRNA abundance of *CX37*, but not that of *epsin 1* and *epsin 2* (Fig. 3C). Consistently, immunofluoresence staining showed that espin 1 and 2 abundance was increased under laminar shear stress, but not under oscillatory shear stress, compared to static condition (Fig. 3D – F, Fig. S8. C, D). These data suggested that *epsin 1* and *epsin 2* gene expression is induced in collecting lymphatic trunk LECs by the initiation of steady lymph flow, but not in valve-covering LECs by oscillatory fluid shear stress.

Epsin and VEGFR3 abundance were inversely correlated during collecting lymphatic vessel development

Maturation of collecting lymphatic vessels is marked by a decrease in collecting lymphatic trunk LECs in the abundance of lymphatic endothelial-specific markers, including VEGFR3, LYVE-1 and Prox1. Failure to decrease the abundance of these markers is linked to defects in the maturation of collecting lymphatic vessels (23). Consistent with previous work (23), whole mount staining revealed high VEGFR3 abundance in collecting lymphatic vessels at E14 and E16 prior to lymphatic valve formation (Fig. 3G). VEGFR3 abundance in collecting lymphatic trunk LECs was considerably decreased during and after lymphatic valve formation, and was maintained at low amounts after birth (Fig. 3H, I). However, VEGFR3 abundance in the valve-covering LECs was not decreased (Fig. 3H, I). Moreover, qRT-PCR analysis of the mesenteric LECs showed that *VEGFR3* mRNA expression did not change during different developmental stages (Fig. S9). In addition, phosphorylation of VEGFR3 was high at E14 and E16, but low after E18 (Fig. 3J) which resulted from increased total VEGFR3 abundance during developmental stages (Fig. 3K). These data suggest temporal and/or spatial regulation of the abundance of VEGFR3 during collecting lymphatic vessel maturation. We next assessed changes in the abundance of epsin 1 and 2

during the development of the collecting lymphatic system. Western blotting analysis showed that the abundance of epsin 1 and 2 in the mesenteric lymphatics was low at E14 to E16, before lymphatic valve formation, but increased at E18 and in postnatal animals (Fig. 3J, K). Thus, the abundance of epsin 1 and 2 in the collecting lymphatic vessels was inversely correlated to that of VEGFR3: the abundance of epsins was high in lymphatic trunk LECs but low in valve-covering LECs, whereas the abundance of VEGFR3 was low in lymphatic trunk LECs but high in valve-covering LECs. These data suggest the possibility of a temporal and spatial relationship between the increase in epsin 1 and 2 abundance and the decrease in VEGFR3 abundance during collecting lymphatic maturation.

Loss of epsins results in the maintenance of high VEGFR3 abundance in lymphatic trunk LECs, leading to lymphatic valve deformation

To investigate whether epsin 1 and 2 play a role in suppressing VEGFR3 abundance in LECs, we examined VEGFR3 abundance in mesenteric collecting lymphatic vessels from P5 wild-type and LEC-DKO pups by whole mount immunofluorescence. VEGFR3 abundance in wild-type collecting lymphatic trunk LECs was low except in the valve-covering LECs (Fig. 4A). In contrast, epsin-deficient LECs did not show a decrease in VEGFR3 abundance resulting in high abundance of this receptor in lymphatic trunk LECs (Fig. 4B). Consistent with these results, Western blotting revealed increased VEGFR3 abundance in LECs purified from the skin (Fig. 4C, D) and mesentery (Fig. 4E, F) of LEC-DKO mice when compared to LECs from WT mice. Intriguingly, loss of epsins in LECs increased the abundance of VEGFR3 but not that of other growth factor receptors including VEGFR1, EGFR, PDGFRβ, or TGFβR1 suggesting that epsin 1 and 2 specifically enhance the abundance of certain receptors (Fig. 4E, F). qRT-PCR analysis indicated that *VEGFR3* mRNA expression in freshly isolated or cultured mesenteric LECs from wild-type or LEC-DKO mice was comparable between the two groups of mice, thus ruling out a role for increased transcription (Fig. S10). Thus, lymphatic valve-covering LECs have high VEGFR3 abundance whereas lymphatic trunk LECs have low VEGFR3 abundance. Epsin 1 and 2, which are induced by steady lymph flow, determine the abundance of VEGFR3 in valve-covering LECs and lymphatic trunk LECs (Fig. 4G). We also examined VEGFR3 abundance in wild-type and LEC-DKO lymphatic capillaries at E16.5 before valve formation and at E18.5 after lymphatic valve formation. VEGFR3 abundance was not statistically different at E16.5 in either genotype (Fig. S3E, S3F, S3J). At E18.5, however, LEC-DKO embryos showed increased VEGFR3 abundance with enlarged lymphatic vessels compared to wild-type embryos (Fig. S3G–H, S3J). We reasoned that the increased VEGFR3 abundance due to epsin deficiency should enhance VEGF-C-induced lymphangiogenesis. To test this notion, we measured lymphatic vessel sprouting and LEC proliferation in the ears of wild-type and LEC-DKO mice after injection of VEGF-C. As expected, VEGF-C adminstration increased numbers of sprouting points and proliferating LECs as revealed by EdU staining in LEC-DKO mice compared to wild-type mice (Fig. S11).

Loss of epsins inhibited ligand-induced VEGFR3 internalization and signaling termination

We have demonstrated that epsins suppress tumor angiogenesis by promoting VEGF-A-induced VEGFR2 internalization and degradation in vascular endothelial cells (31). We

hypothesized that VEGFR3 activated by VEGF-C or VEGF-D also undergoes similar epsin-mediated internalization and degradation to decrease VEGFR3 signaling. To address this question, we measured the cell surface abundance of VEGFR3 on VEGF-C-stimulated primary LECs purified from the skin of wild-type or LEC-DKO mice with anti-podoplanin beads. FACS analysis indicated that after 15 min, VEGF-C stimulation produced a marked decrease in the cell surface pool of VEGFR3 in wild-type LECs, but not in epsin-deficient LECs (Fig. 5A), suggesting that epsins are required for VEGF-C-induced VEGFR3 internalization. In addition, total surface abundance of VEGFR3 was higher in epsin-deficient LECs than in wild-type LECs (Fig. 5A). To further examine whether loss of epsins abolished VEGF-C-induced internalization of cell surface VEGFR3, we performed cell surface biotinylation assays on LECs. After VEGF-C stimulation, a large fraction of VEGFR3 was internalized in wild-type LECs, but not in epsin-deficient LECs (Fig. 5B). These results supported the idea that loss of epsins impairs internalization of cell surface VEGFR3, resulting in surface accumulation of VEGFR3.

To test whether increased cell surface abundance of VEGFR3 affected VEGFR3 signaling, LECs from wild-type or LEC-DKO mice were treated with VEGFC *c156s*, a mutant form of VEGF-C that specifically binds to VEGFR3 but not to VEGFR2 (36, 37). Epsin-deficient LECs had more total and proportionally more phosphorylated VEGFR3 than wild-type LECs (Fig. 5C, D). The phosphorylation of downstream signaling molecules, PLCγ, Akt and ERK, were also significantly higher in epsin-deficient LECs than in wild-type LECs (Fig. 5E, F). These results suggested that epsin 1 and 2 are required for VEGF-C-induced internalization of VEGFR3 and termination of downstream signal transduction processes.

Epsin physically interacted with activated VEGFR3

We next investigated whether epsins interact with VEGFR3. Western blotting of anti-epsin1 immunoprecipitates with anti-VEGFR3 antibody revealed that the interaction of endogenous VEGFR3 with both epsin 1 and epsin 2 was enhanced in primary mouse wild-type skin LECs upon VEGF-C stimulation (Fig. 6A, B). Furthermore, overexpressed VEGFR3 in 293T cells was ubiquitinated after VEGF-C stimulation (Fig. 6C). Because VEGF-C induced the ubiquitination of VEGFR3, we tested whether the interaction of epsin 1 with VEGFR3 requires the ubiquitin interacting motif (UIM). In VEGF-C-stimulated 293T cells, overexpressed VEGFR3 interacted with wild-type epsin 1, but not a mutant form of epsin 1 lacking the UIM domain (epsin 1ΔUIM) (Fig. 6D, E), indicating that the interaction between epsin 1 and activated VEGFR3 requires the epsin UIM.

Deletion of a single VEGFR3 allele or pharmacological suppression of VEGFR3 activity restored lymphatic valve formation and improved lymphatic function caused by epsin loss

Our previous work has established that loss of endothelial epsin 1 and 2 increases VEGFR2 signaling by preventing epsin-mediated internalization of VEGFR2 (31). Deletion of a single VEGFR2 allele improves aberrant VEGFR2 signaling caused by epsin loss (40). In addition to vascular endothelium, VEGFR2 is also present in LECs, and loss of epsin 1 and 2 in LECs also caused increased VEGFR2 abundance (Fig. 4E). Similar to VEGFR3, VEGFR2 is mainly present at lymphatic valve-covering LECs after collecting lymphatic maturation (41). However, the contribution of VEGFR2 to the development of the lymphatic

vascular system has not been defined. We investigated whether specifically reducing the increased VEGFR3 abundance caused by epsin loss would be sufficient to rescue abnormal lymphatic valve formation. We crossed LEC-iDKO mice with VEGFR3-eGFP knock in mice (42), resulting in a VEGFR3 heterozygote on an inducible LEC-specific epsin 1 and 2 deletion background (LEC-iDKO-Flt4 $^{eGFP/+}$). We isolated and purified LECs from wild-type, LEC-iDKO and LEC-iDKO-Flt4 $^{eGFP/+}$ mesenteric tissues. Western blotting indicated that loss of a single *VEGFR3* allele was sufficient to reduce VEGFR3 protein abundance in LEC-iDKO-Flt4 $^{eGFP/+}$ to that of wild-type (Fig. S12A, B). Although LEC-iDKO-Flt4 $^{eGFP/+}$ mice exhibited increased VEGFR2 abundance, the mesenteric lymphatic valve formation and numbers of normal valves were significantly increased and comparable to those wild-type pups at P6 (Fig. 7A–C). Collecting lymphatic drainage function was also improved in LEC-iDKO-Flt4 $^{eGFP/+}$ mice (Fig. 7D, E). To further investigate whether impaired collecting lymphatic valve formation in LEC-DKO mice is a result of sustained VEGFR3 signaling in LECs, we tested whether the VEGFR3 kinase inhibitor MAZ51 (43) could rescue the abnormal lymphatic valve phenotype in LEC-DKO mice. We first determined the effect of MAZ51 on VEGF-C-induced VEGFR3 signaling in SVEC 4-10 cells, a mouse LEC line with endogenous VEGFR3. VEGF-C-induced phosphorylation of VEGFR3 and downstream signaling, as measured by phosphorylation of PLCγ and Akt, were inhibited by MAZ51 treatment (Fig. S12C). Next, we examined if normalization of VEGFR3 signaling by MAZ51 in LEC-DKO pups could restore normal lymphatic development. In skin harvested from P6 pups that were subcutaneously injected with MAZ51 or vehicle control (DMSO), VEGFR3 downstream signaling was decreased by MAZ51 treatment to that seen in wild-type pups (Fig. S12D). Administration of MAZ51 into LEC-DKO pups significantly restored the morphology of collecting lymphatic valves and increased the numbers of mature V-shaped valves at P6 (Fig. 7F, G). Thus, suppression of sustained VEGFR3 signaling increased valve formation in LEC-DKO mice. These data suggest that deletion of a single VEGFR3 allele or pharmacological suppression of sustained VEGFR3 activity increased valve formation in epsin-deficient mice (Fig. 7H). We next analyzed whether administration of MAZ51 also improves the collecting lymphatic drainage function in LEC-DKO pups. We found that MAZ51 treatment improved FITC-Dextran transport through the collecting lymphatic vessels of LEC-DKO pups (Fig. 7I, J). We also examined the lymphatic capillary morphology in both MAZ51 injected LEC-DKO pups and LEC- iDKO-Flt4 $^{eGFP/+}$ pups and found the enlarged lymphatic capillaries in both LEC-DKO and LEC-iDKO pups were restored to sizes comparable to those in wild-type pups (Fig. S13, quantified in Fig. 7K). Collectively, our data demonstrated a role for epsins in promoting the crucial function of collecting lymphatic vessels by temporal and spatial reducing VEGFR3 abundance, and thus VEGFR3 signaling, resulting in normal valve formation during embryonic and early postnatal life.

DISCUSSION

Our findings have unraveled a crucial role of epsins in regulating collecting lymphatic development by controlling lymphatic valve formation and drainage function. The mechanical stimulus caused by lymph flow greatly increased epsin 1 and 2 abundance in lymphatic trunk LECs before collecting lymphatic valve formation. Epsin 1 and 2

functioned as inhibitors of VEGFR3 by mediating the degradation of this receptor, which resulted in the establishment of LECs with low abundance of VEGFR3 in collecting lymphatic trunks. In contrast, VEGFR3 abundance remained high in regions with low epsin abundance, namely at valve-covering regions (Fig. S14). Thus, epsins regulate lymphatic endothelial cell behavior by dampening the VEGFR3 signaling pathway, like Rasa 1, another inhibitor of VEGFR3 signaling (44). Similar to epsins, Ephrin-B2 also control the growth of blood and lymphatic vessels but do so by promoting the endosomal localization of VEGFR2 and VEGFR3, thereby promoting VEGFR2 and VEGFR3 signaling (45, 46).

Lymphatic capillary patterning and lymphovenous valves developed normally in epsin-deficient embryos at early developmental stage. Normal lymphovenous valve formation and lymphatic capillary development ensure functional drainage in early stage embryos and explains the absence of edema in LEC-DKO embryos. Conversely, we observed that epsin deficiency caused dilation of collecting lymphatic vessels and lymphatic capillaries in E18.5 embryos and neonates. However, prominent dilation in lymphatic capillaries and major defects were not apparent in collecting lymphatic patterning before lymphatic valve formation, suggesting that the impaired lymphatic valves is unlikely a secondary defects caused by dilated vessels at early developmental stages. In addition to collecting lymphatics, VEGFR3 abundance was also increased in dilated lymphatic capillaries in E18.5 LEC-DKO embryos. Whether the dilation of lymphatic vessels is a direct result of increased VEGFR3 signaling or a secondary by product of impaired lymphatic drainage still needs to be investigated fully in the future. Furthermore, how epsin abundance is regulated in lymphatic capillary needs to be determined.

Dysfunction in lymphatic vessels is implicated in numerous human diseases including lymphedema, inflammation and cancer metastasis. Effective treatments for edema or metabolic diseases due to collecting lymphatic dysfunction are currently lacking. Patients with Lymphedema-Distichiasis Syndrome carry mutations in the forkhead transcription factor Foxc2. Mice with Foxc2 deficiency display defective lymphatic valve formation and maturation. Together, they provide evidence that lymphatic valves play critical roles in maintaining unidirectional flow and preventing lymph back flow (13). Understanding the mechanisms underlying lymphatic valve formation will help generate new therapeutic strategies that target lymphatic valve malformation or collecting lymphatic dysfunction. Our work suggests that epsins regulate lymphatic valve development and function and could be potential therapeutic targets.

MATERIALS AND METHODS

Animal model

All animal procedures were approved by the Institutional Animal Care and Use Committee of the Oklahoma Medical Research Foundation.

We have reported a strategy for generation of an epsin 1 and 2 global DKO mouse model (29, 31). Briefly, *Epsin 1*$^{fl/fl}$ mice were mated with *epsin 2*$^{-/-}$ mice to generate *epsin 1*$^{fl/fl}$; *epsin 2*$^{-/-}$ mice. *LYVE-1 EGFP*-hCre mice were purchased from Jackson Laboratory (Bar Harbor, ME) and have the LYVE-1 promoter driving constitutive expression of Cre

recombinase in LECs (47). Constitutive LEC-specific epsin 1 and 2 deletion (LEC-DKO) mice were generated by crossing *epsin 1*$^{fl/fl}$*; epsin 2*$^{-/-}$ mice with *LYVE-1 EGFP*-hCre mice that specifically delete epsin 1 and 2 in LECs (47). *Prox1-CreER*^{T2} deleter mouse was a kind gift from Dr. R. Sathish Srinivasan and has been described previously (48). Tamoxifen inducible LEC-specific epsin 1 and 2 deletion (LEC-iDKO) mice were obtained by crossing *epsin 1*$^{fl/fl}$*; epsin 2*$^{-/-}$ mice with *Prox1-CreER*^{T2} deleter mice which inactivate the epsin 1 gene specifically in LECs cells upon tamoxifen administration. VEGFR3-eGFP knock-in mouse was a kind gift from Dr. Hirotake Ichise and has been described previously (40). VEGFR3 heterozygous LEC-iDKO mice (LEC-iDKO-Flt4$^{eGFP/+}$) were generated by crossing *epsin 1*$^{fl/fl}$; *epsin 2*$^{-/-}$ mice with VEGFR3-Egfp mice generating *epsin 1*$^{fl/fl}$; *epsin 2*$^{-/-}$; *Flt4*$^{eGFP/+}$ mice, then subsequently crossing with *Prox1-CreER*^{T2} deleter mice. All mice were bred on C57BL/6J background. To induce embryonic deletion of epsin 1, we administered 4-hydroxytamoxifen (50 μg per 10g of body weight) by intraperitoneal injection into pregnant females at E11 and E12. To induce postnatal deletion of epsin 1, we administered 4-hydroxytamoxifen by intraperitoneal injection into pregnant mice using the dose above at E14 then 50 μg was injected into pups at P3, P4 and P5. Embryonic age (E) was determined according to the day of the vaginal plug (E0.5).

Visualization of lymphatic vessels function

To examine mouse ear lymphatic drainage, 5 μL of 8 mg/mL FITC-Dextran (2,000kDa, Sigma) was intradermally injected into P14 mouse ears. Fifteen minutes post-injection, mice were euthanized. Ears were removed and fixed in 4% paraformaldehyde (PFA). To examine the mouse hind leg lymphatic drainage, 5 μL of 8 mg/mL FITC-Dextran or 8 μL of 3% Evans blue dye (Sigma-Aldrich) was intradermally injected into mouse foot pads. Fifteen minutes post-injection, mice were euthanized. For FITC-Dextran injected mice, the hind leg skin was removed and fixed in 4% PFA. FITC-Dextran transport was visualized by an Olympus IX81 Spinning Disc Confocal Microscope with an Olympus plan Apo Chromat 10x objective and Hamamatsu Orca-R2 Monochrome Digital Camera at room temperature. To investigate the mouse tail lymphatic vessel function, 10 μL of 8 mg/mL FITC-Dextran was injected into mouse tail tip. The FITC-Dextran reflux was examined by Olympus BH-2 intravital multiphoton microscope with Zeiss Axiocam MRC camera and the fluorescent intensity was analyzed by Zeiss Axovision 4.8 software. For Evans blue injected mice, popliteal lymph nodes were dissected and the Evans blue-stained popliteal lymph nodes were imaged by a CCD camera attached to a stereo-microscope (Leica). Color intensities were compared.

Lymphatic vessel sprouting and proliferation in vivo

To detect lymphatic vessel sprouting in vivo, 3-month-old wild-type and LEC-DKO mice was daily treated with 100 ng of recombinant VEGF-C (R&D) in PBS or PBS by intradermal injection into the ear skin for 2 days. To detect lymphatic endothelial proliferation, mice were injected intraperitoneally with 150 μg EdU (Sigma) in PBS at day 2 after VEGF-C injections. At day 3, mice were killed and one ear of each mouse was dissected for whole mount staining. The other ear was embedded in optimal cutting temperature (OCT) compound (Sakura).

Immunostaining

For tissue whole mount staining, mesentery, intestine, or skin were dissected, fixed in 4% PFA, and blocked in PBS solution containing 5% donkey serum and 0.3% Triton X-100. For staining, we used anti-mouse CD31 (BD), anti-mouse VEGFR3 (R&D), anti-mouse LYVE-1 (R&D), anti-mouse Neuropilin-2 (R&D), anti-mouse integrinα-9 (R&D), goat anti-mouse epsin 1 (Santa Cruz), goat anti-mouse epsin 2 (Santa Cruz), and anti-mouse Prox1 (Angiobio) antibodies. Samples were mounted with Vectashield. Photomicrographs were obtained using an Olympus IX81 Spinning Disc Confocal Microscope with an Olympus plan Apo Chromat 20x objective and Hamamatsu Orca-R2 Monochrome Digital Camera.

For OCT embedded ear tissues, 10-μm cryostat sections were cut, air dried, fixed in 4% PFA, and blocked in PBS solution containing 5% donkey serum and 0.3% Triton X-100. We used anti-mouse LYVE-1 (R&D) antibodies for staining. In the case of EdU labeling, sections after incubation with secondary antibodies were fixed in 4% PFA for 20 min and incorporated EdU was detected by incubation with 100 μM Alexa Fluor 594 azide (Life technologies) diluted in 100 mM Tris, 0.5 mM CuSO4 and 50 mM ascorbic acid. Samples were mounted and analyzed as described above.

For LEC staining, cultured LECs were fixed with 4% PFA or 100% MetOH, permeabilized with 0.1% Triton X-100 and blocked in PBS solution containing 5% donkey serum and 0.1% Triton X-100. We used anti-LYVE-1 antibody to analyze LEC purification. We used rabbit anti-epsin 1 (26, 27) and goat anti-epsin 2 (Santa Cruz) antibodies to measure epsin 1 and 2 abundance under flow or static conditions. Samples were mounted and analyzed as described above.

Cell culture, plasmids and transfection

Primary mouse LECs were isolated from skin or mesenteric tissues of wild-type and LEC-DKO mice as previously described (49). Briefly, the finely minced skin or mesentery tissue was digested with enzyme solution (2 mg/ml collagenase, 5 mg/ml dispase; Roche) at 37°C for 1 hour, then the cells were cultured in complete endothelial cell medium (Invitrogen). Anti-Podoplanin antibody (clone 8F11, MBL) was first labeled with Biotin (EZ-Link® Micro Sulfo-NHS-LC Biotinylation Kit) according to the manufacture's instructions. LECs were further purified by streptavidin-conjugated magnetic beads (Pierce) after cells were incubated with biotinylated anti-Podoplanin antibodies for 2 hours at room temperature. The identity of LECs was confirmed with LYVE-1 immunofluorescence staining and VEGFR3 flow cytometry analysis. LEC purity (>90%) was measured by expressions of LYVE-1 and VEGFR3. Deletion of epsin 1 and 2 were confirmed by quantitative RT-PCR and Western blotting.

Mammalian expression plasmids for HA-tagged epsin 1 and its mutants were described previously (28). 293T cells were transfected with VEGFR3, HA-tagged epsin 1, or HA-tagged epsin1ΔUIM constructs with Lipofectamine 2000 according to the manufacturer's instructions (Invitrogen).

RNA extraction and Quantitative RT-PCR

Mouse LECs were isolated and purified as described. Mesenteric tissues were harvested from P6 wild-type or LEC-DKO mice. RNA was extracted using RNeasy Mini Kit (QIAGEN) according to the manufacturer's instructions. cDNA was synthesized using the SuperScript III First-Strand Synthesis SuperMix (Invitrogen). Individual quantitative RT-PCR was performed using gene-specific primers. VEGFR3 (5′-CTGGCCAGAGGCACTAAGAC-3′, 5′-CAGGGTGTCCTCTGGGAATA-3′) (50); Epsin 1 (5′-CTACCAACGTCCATTGCGGT-3′, 5′-GCAGCGATGAGGTCGACATT-3′); Epsin 2 (5′-TCT ATC AGA CGG CAG ATG AAA AAC-3′, 5′-GTC ATT GGA GGT GGC CTC C-3′); CX37 (5′-GGCTGGACCATGGAGCCGGT-3′, 5′-TTTCGGCCACCCTGGGGAGC-3′); 18S rRNA (5′-CGCGGTCCTATTCCATTATTC-3′, 5′-CCC GAA GCG TTT ACT TTG AAA-3′).

Immunoprecipitation and Western Blotting

Immunoprecipitation and Western blotting analyses were performed as described previously (31). For detection of phosphorylated VEGFR3 signaling *in vitro*, LECs were lysed with RIPA buffer (25mM Tris-HCl pH 7.6, 150 mM NaCl, 1% NP-40, 1% sodium deoxycholate, 0.1% SDS at pH6.8 and protease inhibitors) after stimulation with 100 ng/ml VEGFC *c156s* (R&D) for 0, 5, and 15 minutes. Cell lysates were followed by immunoprecipitation with anti-mouse VEGFR3 antibodies (R&D) and Western blotting using anti-mouse 4G10 antibodies (Santa Cruz). Ligand induced downstream signaling were detected by Western blotting using antibodies against p-Akt (Cell Signaling), p-PLCγ (Cell Signaling), p-ERK (Cell Signaling).

For detection of the endogenous interaction of VEGFR3 with epsin 1 or epsin 2, LECs were lysed with RIPA buffer after stimulation with 100 ng/ml VEGF-C (R&D) for 0, 5, and 15 minutes. Cell lysates were followed by immunoprecipitation with goat anti-mouse epsin 1 (Santa Cruz) or epsin 2 (Santa Cruz) antibodies and Western blotting using VEGFR3 antibodies (R&D).

Skin or mesentery tissues from P6 wild-type or LEC-DKO mice were dissected and sonicated in RIPA buffer. Total protein concentration was measured using the BCA Protein Assay Kit (Pierce). Western blot analyses were performed using anti-VEGFR3 (R&D), anti-VEGFR2 (Cell Signaling), anti-VEGFR1 (Cell Signaling), anti-TGFβR1 (Cell Signaling), anti-PDGFRβ (Cell Signaling), or anti-EGFR (Cell Signaling) antibodies. All Western blotting quantification was performed by NIH Image 1.60.

For mesenteric LECs Western blotting, mesenteric tissues were dissected from E14, E16, E18, P0, and P6 embryos or pups. Collecting lymphatics from E16, E18, P0, and P6 were carefully collected from mesenteric tissues under dissection microscopy. Tissues were digested and LECs were purified as described above. Protein abundance were detected by Western blotting using anti-mouse epsin 1 (26, 27), anti-mouse epsin 2 (27), anti-mouse VEGFR3 (R&D) and anti-mouse p-VEGFR3 (Cell Applications) antibodies.

For detecting the interactions of VEGFR3 with epsin 1 UIM domain, lysates of transfected 293T cells were either pulled down by anti-HA antibodies (epsin 1 or epsin 1ΔUIM), or

anti-human VEGFR3 antibodies (Cell Signaling). Interactions were identified by Western blotting using anti-human VEGFR3 (Cell Signaling) or anti-HA (Roche) antibodies. For Western blotting, bound antibodies were detected using HRP-conjugated secondary antibodies (Jackson ImmunoResearch) and ECL chemiluminescence (Pierce).

Cell surface VEGFR3 endocytosis assay

Mouse LEC cell surface VEGFR3 endocytosis was performed as described previously (31). Briefly, mouse LECs were incubated with 1 mM EZ-Link Sulfo-NHS-S-S-Biotin (Pierce) on ice for 30 minutes. Cells were then stimulated with 100 ng/ml VEGF-C for 0, 5, and 15 minutes to allow receptor endocytosis. Remaining uninternalized surface biotinylated plasma membrane proteins were removed by incubation with PBS/50 mM glycine/50 mM DTT for 30 minutes on ice. Cells were lysed and processed for streptavidin bead pull down. Internalized VEGFR3 was visualized by Western blotting using anti-VEGFR3 antibodies and quantified by NIH Image 1.60.

FACS analysis of cell surface abundance of VEGFR3

FACS analysis of the cell surface abundance of VEGFR3 was performed as described previously (31). Briefly, mouse LEC suspensions were stained with anti-VEGFR3 antibody (R&D) for 30 minutes on ice, followed by fluorescent secondary antibody staining for another 30 minutes on ice. Isotype antibody served as a negative control. Flow cytometry was performed on a FACSCalibur (BD Biosciences). Data were analyzed with BD CellQuest Pro software.

Application of shear stress to LEC monolayers

To examine effect of shear stress on epsin mRNA and protein abundance in LECs, LECs were cultured in a parallel flow chamber (ibidi flow chamber, ibidi) under laminar shear flow (4 dyn/cm^2) or under oscillatory flow conditions (4 dyn/cm^2, ¼ HZ) driven by a peri-static pump as described previously (12), or under static condition for 16 hr at 37 °C. Shear stress parameters were chosen based on the stress measurements reported previously (11). Some sets of LECs were pretreated with 10 μM PP2 (4-amino-5-(4-chlorophenyl)-7-(t-butyl) pyrazolo [3, 4-d]pyrimidine) (Sigma-Aldrich), a Src family kinase inhibitor, or DMSO for 30 min before exposure to laminar shear flow as described previously (51).

Administration of the VEGFR3 pharmacological inhibitor MAZ51

The SVEC 4-10 cell line, an SV40-transformed murine endothelial cell line (52), was a kind gift from Dr. Minghui Zhou. For *in vitro* experiment, LECs were further purified from SVEC 4-10 by streptavidin-conjugated magnetic beads after cells were incubated with biotinylated anti-podoplanin antibody. Purified SEVC 4-10 cells were starved overnight and pretreated with 10 μM MAZ51 (Sigma-Aldrich) for 4 hours, followed by VEGF-C stimulation for 5 minutes. For in vivo experiment, 10 mg/kg MAZ51 or DMSO was subcutaneously injected into LEC-DKO pups at P2, P5, and 8h before dissection at P6 as described previously (43).

Statistical analysis

Percentages dependence on covariates was modeled with logistic regression implemented as part of glm function in the R statistical software. Distribution of continuous variable means (for example, mean expression) among several groups was analyzed with the ANOVA procedure or t test also implemented in R. Validity of the ANOVA assumptions was established with Shapiro-Wilks test (normality) and Brown-Forsythe Levene test (homoscedasticity). The 95% confidence intervals of group means/proportions, shown in the figures, were returned by the glm/ANOVA procedures as part of the standard output. The p values for testing the difference between groups, also displayed in the figures, were obtained by using the contrast options of the two functions. The omnibus test, implemented as part of ANOVA, was used to test mean equality among several groups at once.

Supplementary Material

Refer to Web version on PubMed Central for supplementary material.

Acknowledgments

We thank Dr. Rodger McEver and Dr. Ralf H. Adams for insightful comments and helpful discussions. We thank the OMRF imaging core for help with the presentation of figures.

FUNDING: This work was supported in part by NIH grants R01HL-093242, P20 RR018758, a grant from the Oklahoma Center for Advanced Science and Technology (OCAST), a National Scientific Development Grant from the American Heart Association (0835544N), and a grant from Department of Defense W81XWH-11-1-00226 to H. Chen, by NIH grant P01HL085607 to L. Xia, by grants from Oklahoma Center for Advanced Science and Technology (AR11-043) and the American Heart Association (12SDG8760002) to Y. Dong, by a predoctoral fellowship from the American Heart Association (RSRCH016952) to X. Liu, by AHA postdoctoral fellowships 13POST16940008 to K. L. Tessneer, and 13POST17270006 to S. Pasula.

REFERENCES AND NOTES

1. Karpanen T, Alitalo K. Molecular biology and pathology of lymphangiogenesis. Annu Rev Pathol. 2008; 3:367–97. [PubMed: 18039141]
2. François M, Caprini A, Hosking B, Orsenigo F, Wilhelm D, Browne C, Paavonen K, Karnezis T, Shayan R, Downes M, Davidson T, Tutt D, Cheah KS, Stacker SA, Muscat GE, Achen MG, Dejana E, Koopman P. Sox18 induces development of the lymphatic vasculature in mice. Nature. 2008; 456:643–7. [PubMed: 18931657]
3. Lin FJ, Chen X, Qin J, Hong YK, Tsai MJ, Tsai SY. Direct transcriptional regulation of neuropilin-2 by COUP-TFII modulates multiple steps in murine lymphatic vessel development. J Clin Invest. 2010; 120:1694–707. [PubMed: 20364082]
4. Wigle JT, Oliver G. Prox1 function is required for the development of the murine lymphatic system. Cell. 1999; 98:769–78. [PubMed: 10499794]
5. Srinivasan RS, Oliver G. Prox1 dosage controls the number of lymphatic endothelial cell progenitors and the formation of the lymphovenous valves. Genes Dev. 2011; 25:2187–97. [PubMed: 22012621]
6. Schulte-Merker S, Sabine A, Petrova TV. Lymphatic vascular morphogenesis in development, physiology, and disease. J Cell Biol. 2011; 193:607–18. [PubMed: 21576390]
7. Tammela T, Alitalo K. Lymphangiogenesis: Molecular mechanisms and future promise. Cell. 2010; 140:460–76. [PubMed: 20178740]
8. Uhrin P, Zaujec J, Breuss JM, Olcaydu D, Chrenek P, Stockinger H, Fuertbauer E, Moser M, Haiko P, Fässler R, Alital K, Binder BR, Kerjaschki D. Novel function for blood platelets and podoplanin in developmental separation of blood and lymphatic circulation. Blood. 2010; 115:3997–4005. [PubMed: 20110424]

9. Bertozzi CC, Schmaier AA, Mericko P, Hess PR, Zou Z, Chen M, Chen CY, Xu B, Lu MM, Zhou D, Sebzda E, Santore MT, Merianos DJ, Stadtfeld M, Flake AW, Graf Y, Skoda R, Maltzman JS, Koretzky GA, Kahn ML. Platelets regulate lymphatic vascular development through CLEC-2-SLP-76 signaling. Blood. 2010; 116:661–70. [PubMed: 20363774]
10. Maby-El Hajjami H, Petrova TV. Developmental and pathological lymphangiogenesis: from models to human disease. Histochem Cell Biol. 2008; 130:1063–78. [PubMed: 18946678]
11. Zawieja DC. Contractile physiology of lymphatics. Lymphat Res Biol. 2009; 7:87–96. [PubMed: 19534632]
12. Sabine A, Agalarov Y, Maby-El Hajjami H, Jaquet R, Hägerling M, Pollmann C, Bebber D, Pfenniger A, Miura N, Dormond O, Calmes JM, Adams RH, Mäkinen T, Kiefer F, Kwak BR, Petrova TV. Mechanotransduction, PROX1, and FOXC2 cooperate to control connexin37 and calcineurin during lymphatic-valve formation. Dev Cell. 2012; 22:430–45. [PubMed: 22306086]
13. Petrova TV, Karpanen T, Norrmén C, Mellor R, Tamakoshi T, Finegold D, Ferrell R, Kerjaschki D, Mortimer P, Ylä-Herttuala S, Miura N, Alitalo K. Defective valves and abnormal mural cell recruitment underlie lymphatic vascular failure in lymphedema distichiasis. Nat Med. 2004; 10:974–81. [PubMed: 15322537]
14. Mäkinen T, Adams RH, Bailey J, Lu Q, Ziemiecki A, Alitalo K, Klein R, Wilkinson GA. PDZ interaction site in ephrinB2 is required for the remodeling of lymphatic vasculature. Genes Dev. 2005; 19:397–410. [PubMed: 15687262]
15. Kanady JD, Dellinger MT, Munger SJ, Witte MH, Simon AM. Connexin37 and Connexin43 deficiencies in mice disrupt lymphatic valve development and result in lymphatic disorders including lymphedema and chylothorax. Dev Biol. 2011; 354:253–66. [PubMed: 21515254]
16. Jurisic G, Maby-El Hajjami H, Karaman S, Ochsenbein AM, Alitalo A, Siddiqui SS, Ochoa Pereira C, Petrova TV, Detmar M. An unexpected role of semaphorin3a-neuropilin-1 signaling in lymphatic vessel maturation and valve formation. Circ Res. 2012; 111:426–36. [PubMed: 22723300]
17. Bouvrée K, Brunet I, Del Toro R, Gordon E, Prahs C, Cristofaro B, Mathivet T, Xu Y, Soueid J, Fortuna V, Miura N, Aigrot MS, Maden CH, Ruhrberg C, Thomas JL, Eichmann A. Semaphorin3A, Neuropilin-1, and PlexinA1 are required for lymphatic valve formation. Circ Res. 2012; 111:437–45. [PubMed: 22723296]
18. Bazigou E, Xie S, Chen C, Weston A, Miura N, Sorokin L, Adams R, Muro AF, Sheppard D, Makinen T. Integrin-alpha9 is required for fibronectin matrix assembly during lymphatic valve morphogenesis. Dev Cell. 2009; 17:175–86. [PubMed: 19686679]
19. Levet S, Ciais D, Merdzhanova G, Mallet C, Zimmers TA, Lee SJ, Navarro FP, Texier I, Feige JJ, Bailly S, Vittet D. Bone morphogenetic protein 9 (BMP9) controls lymphatic vessel maturation and valve formation. Blood. 2013; 122:598–607. [PubMed: 23741013]
20. Alitalo K, Tammela T, Petrova TV. Lymphangiogenesis in development and human disease. Nature. 2005; 438:946–53. [PubMed: 16355212]
21. Alitalo K. The lymphatic vasculature in disease. Nat Med. 2011; 17:1371–80. [PubMed: 22064427]
22. Harvey NL. The link between lymphatic function and adipose biology. Ann N Y Acad Sci. 2008; 1131:82–8. [PubMed: 18519961]
23. Norrmén C, Ivanov KI, Cheng J, Zangger N, Delorenzi M, Jaquet M, Miura N, Puolakkainen P, Horsley V, Hu J, Augustin HG, Ylä-Herttuala S, Alitalo K, Petrova TV. FOXC2 controls formation and maturation of lymphatic collecting vessels through cooperation with NFATc1. J Cell Biol. 2009; 185:439–57. [PubMed: 19398761]
24. Karkkainen MJ, Haiko P, Sainio K, Partanen J, Taipale J, Petrova TV, Jeltsch M, Jackson DG, Talikka M, Rauvala H, Betsholtz C, Alitalo K. Vascular endothelial growth factor C is required for sprouting of the first lymphatic vessels from embryonic veins. Nat Immunol. 2004; 5:74–80. [PubMed: 14634646]
25. Dumont DJ, Jussila L, Taipale J, Lymboussaki A, Mustonen T, Pajusola K, Breitman M, Alitalo K. Cardiovascular failure in mouse embryos deficient in VEGF receptor-3. Science. 1998; 282:946–9. [PubMed: 9794766]

26. Chen H, Fre S, Slepnev VI, Capua MR, Takei K, Butler MH, Di Fiore PP, De Camilli P. Epsin is an EH-domain-binding protein implicated in clathrin-mediated endocytosis. Nature. 1998; 394:793–7. [PubMed: 9723620]
27. Rosenthal JA, Chen H, Slepnev VI, Pellegrini L, Salcini AE, Di Fiore PP, De Camilli P. The epsins define a family of proteins that interact with components of the clathrin coat and contain a new protein module. J Biol Chem. 1999; 274:33959–65. [PubMed: 10567358]
28. Chen H. From the Cover: The association of epsin with ubiquitinated cargo along the endocytic pathway is negatively regulated by its interaction with clathrin. Proc Natl Acad Sci. 2005; 102:2766–2771. [PubMed: 15701696]
29. Chen H, Ko G, Zatti A, Di Giacomo G, Liu L, Raiteri E, Perucco E, Collesi C, Min W, Zeiss C, De Camilli P, Cremona O. Embryonic arrest at midgestation and disruption of Notch signaling produced by the absence of both epsin 1 and epsin 2 in mice. Proc Natl Acad Sci U S A. 2009; 106:13838–43. [PubMed: 19666558]
30. Ko G, Paradise S, Chen H, Graham M, Vecchi M, Bianchi F, Cremona O, Di Fiore PP, De Camilli P. Selective high-level expression of epsin 3 in gastric parietal cells, where it is localized at endocytic sites of apical canaliculi. Proc Natl Acad Sci U S A. 2010; 107:21511–6. [PubMed: 21115825]
31. Pasula S, Cai X, Dong Y, Messa M, McManus J, Chang B, Liu X, Zhu H, Mansat RS, Yoon SJ, Hahn S, Keeling L, Saunders D, Ko G, Knight J, Newton G, Luscinskas F, Sun X, Towner R, Lupu F, Xia L, Cremona O, De Camilli P, Min W, Chen H. Endothelial epsin deficiency decreases tumor growth by enhancing VEGF signaling. J Clin Invest. 2012; 122:4424–38. [PubMed: 23187125]
32. Carramolino L, Fuentes J, García-Andrés C, Azcoitia V, Riethmacher D, Torres M. Platelets play an essential role in separating the blood and lymphatic vasculatures during embryonic angiogenesis. Circ Res. 2010; 106:1197–201. [PubMed: 20203303]
33. Ji RC. Lymphatic endothelial cells, lymphedematous lymphangiogenesis, and molecular control of edema formation. Lymphat Res Biol. 2008; 6:123–37. [PubMed: 19093784]
34. Xu Y, Yuan L, Mak J, Pardanaud L, Caunt M, Kasman I, Larrivée B, Del Toro R, Suchting S, Medvinsky A, Silva J, Yang J, Thomas JL, Koch AW, Alitalo K, Eichmann A, Bagri A. Neuropilin-2 mediates VEGF-C-induced lymphatic sprouting together with VEGFR3. J Exp Med. 2010; 207:115–130. S1–S7.
35. Resnick N, Yahav H, Shay-Salit A, Shushy M, Schubert S, Zilberman LCM, Wofovitz E. Fluid shear stress and the vascular endothelium: for better and for worse. Prog Biophys Mol Biol. 2003; 81:177–199. [PubMed: 12732261]
36. Ng CP, Helm CLE, Swartz MA. Interstitial flow differentially stimulates blood and lymphatic endothelial cell morphogenesis in vitro. Microvasc Res. 2004; 68:258–64. [PubMed: 15501245]
37. Okuda M, Takahashi M, Suero J, Murry CE, Traub O, Kawakatsu H, Berk BC. Shear stress stimulation of p130(cas) tyrosine phosphorylation requires calcium-dependent c-Src activation. J Biol Chem. 1999; 274:26803–26809. [PubMed: 10480886]
38. Veikkola T, Jussila L, Makinen T, Karpanen T, Jeltsch M, Petrova TV, Kubo H, Thurston G, McDonald DM, Achen MG, Stacker SA, Alitalo K. Signalling via vascular endothelial growth factor receptor-3 is sufficient for lymphangiogenesis in transgenic mice. EMBO J. 2001; 20:1223–31. [PubMed: 11250889]
39. Joukov V, Kumar V, Sorsa T, Arighi E, Weich H, Saksela O, Alitalo K. A recombinant mutant vascular endothelial growth factor-C that has lost vascular endothelial growth factor receptor-2 binding, activation, and vascular permeability activities. J Biol Chem. 1998; 273:6599–602. [PubMed: 9506953]
40. Tessneer L, Pasula S, Cai X, Dong Y, McManus J, Liu X, Yu L, Hahn S, Chang B, Chen Y, Griffin C, Xia L, Adams RH, Chen H. Genetic reduction of vascular endothelial growth factor receptor 2 rescues aberrant angiogenesis caused by epsin deficiency. Arterioscler Thromb Vasc Biol. 2014; 34:331–7. [PubMed: 24311377]
41. Wirzenius M, Tammela T, Uutela M, He Y, Odorisio T, Zambruno G, Nagy JA, Dvorak HF, Ylä-Herttuala S, Shibuya M, Alitalo K. Distinct vascular endothelial growth factor signals for lymphatic vessel enlargement and sprouting. J Exp Med. 2007; 204:1431–40. [PubMed: 17535974]

42. Ichise T, Yoshida N, Ichise H. H-, N- and Kras cooperatively regulate lymphatic vessel growth by modulating VEGFR3 expression in lymphatic endothelial cells in mice. Development. 2010; 137:1003–13. [PubMed: 20179099]
43. Benedito R, Rocha SF, Woeste M, Zamykal M, Radtke F, Casanovas O, Duarte A, Pytowski B, Adams RH. Notch-dependent VEGFR3 upregulation allows angiogenesis without VEGF-VEGFR2 signalling. Nature. 2012; 484:110–4. [PubMed: 22426001]
44. Lapinski PE, Kwon S, Lubeck BA, Wilkinson JE, Srinivasan RS, Sevick-Muraca E, King PD. RASA1 maintains the lymphatic vasculature in a quiescent functional state in mice. J Clin Invest. 2012; 122:733–47. [PubMed: 22232212]
45. Wang Y, Nakayama M, Pitulescu ME, Schmidt TS, Bochenek ML, Sakakibara A, Adams S, Davy A, Deutsch U, Lüthi U, Barberis A, Benjamin LE, Mäkinen T, Nobes CD, Adams RH. Ephrin-B2 controls VEGF-induced angiogenesis and lymphangiogenesis. Nature. 2010; 465:483–6. [PubMed: 20445537]
46. Sawamiphak S, Seidel S, Essmann CL, Wilkinson GA, Pitulescu ME, Acker T, Acker-Palmer A. Nature. 2010; 465:487–91. [PubMed: 20445540]
47. Pham THM, Baluk P, Xu Y, Grigorova I, Bankovich AJ, Pappu R, Coughlin SR, McDonald DM, Schwab SR, Cyster JG. Lymphatic endothelial cell sphingosine kinase activity is required for lymphocyte egress and lymphatic patterning. J Exp Med. 2010; 207:17–27. [PubMed: 20026661]
48. Srinivasan RS, Dillard ME, Lagutin OV, Lin FJ, Tsai S, Tsai MJ, Samokhvalov IM, Oliver G. Lineage tracing demonstrates the venous origin of the mammalian lymphatic vasculature. Genes Dev. 2007; 21:2422–32. [PubMed: 17908929]
49. Kriehuber E, Breiteneder-Geleff S, Groeger M, Soleiman A, Schoppmann SF, Stingl G, Kerjaschki D, Maurer D. Isolation and characterization of dermal lymphatic and blood endothelial cells reveal stable and functionally specialized cell lineages. J Exp Med. 2001; 194:797–808. [PubMed: 11560995]
50. Kazenwadel J, Michael MZ, Harvey NL. Prox1 expression is negatively regulated by miR-181 in endothelial cells. Blood. 2010; 116:2395–401. [PubMed: 20558617]
51. Jin ZG, Wong C, Wu J, Berk BC. Flow shear stress stimulates Gab1 tyrosine phosphorylation to mediate protein kinase B and endothelial nitric-oxide synthase activation in endothelial cells. J Biol Chem. 2005; 280:12305–9. [PubMed: 15665327]
52. O'Connell KA, Edidin M. A mouse lymphoid endothelial cell line immortalized by simian virus 40 binds lymphocytes and retains functional characteristics of normal endothelial cells. J Immunol. 1990; 144:521–5. [PubMed: 2153170]

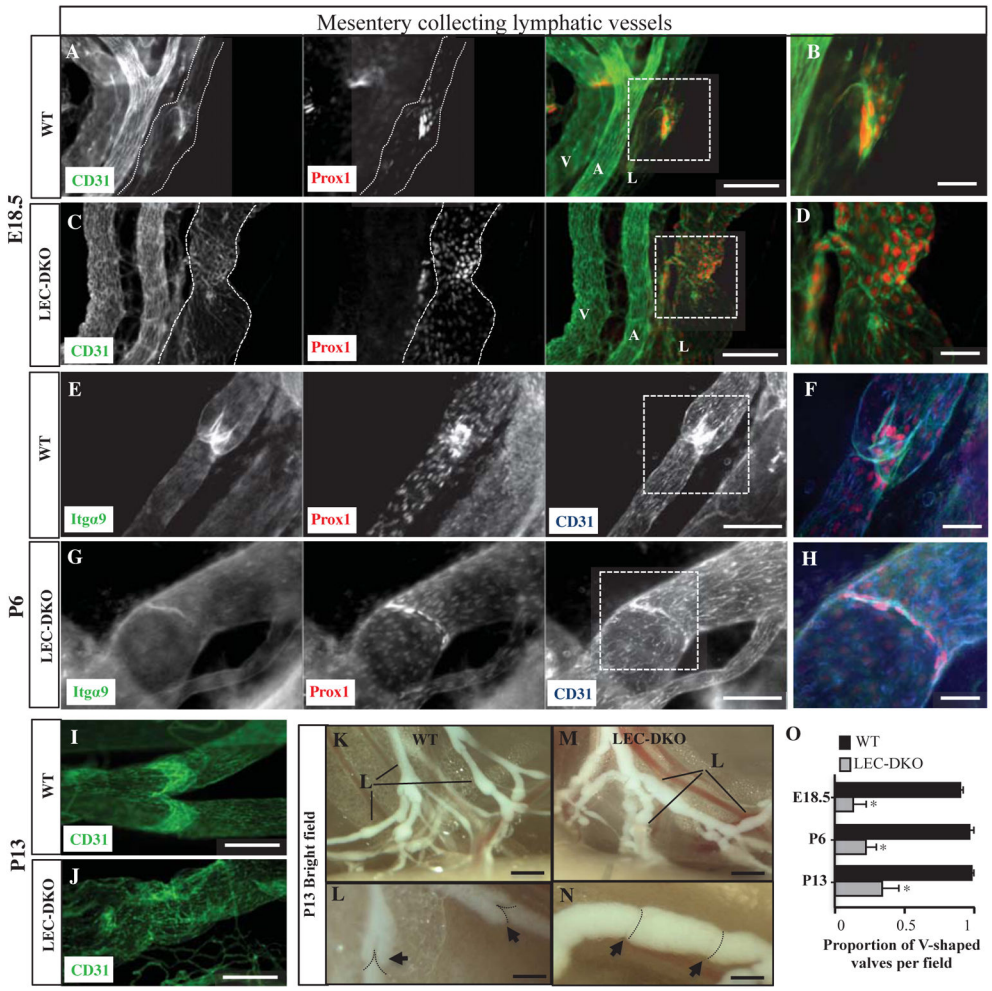

Fig. 1. Defective collecting lymphatic valve formation in LEC-DKO mice

A–H) Representative whole mount immunofluorescent staining of wild-type and LEC-DKO mesenteric lymphatic valves at E18.5 (A–D) and P6 (E–H) with antibodies against CD31, Prox1 and Integrin-α9. B, D and F, H are enlarged images of A, C and E, G. A, C: n=5 embryos per group; E, G: n=6 pups per group. Itgα9: Integrin-α9. V: vein, A: artery, L: collecting lymphatic. Scale bar, 100 μm (A, C, E, G); Scale bar, 50 μm (B, D, F, H). **I–J)** Representative whole mount immunofluorescent staining of wild-type (I) and LEC-DKO (J) mesenteric lymphatic valves at P13 with antibodies against CD31 (n=6 pups per group). Scale bar, 100 μm. **K–N**) Representative bright field images of chyle-filled mesenteric vessels in both wild-type (K, L) and LEC-DKO mice (M, N) (n=6 mice per group). LEC-DKO mice (L) have immature valve morphology (black arrow) and dilated vessels compared to wild-type mice (N). L: Lymphatic vessels. Scale bar, 1 mm (K–M); Scale bar, 50 μm (L–N). **O**) Quantification of percentages of V-shaped valve numbers of in wild-type and LEC-DKO mice at different developmental stages. *, P<0.05; geographic regression. All values are mean ± SD (n=3 independent experiments).

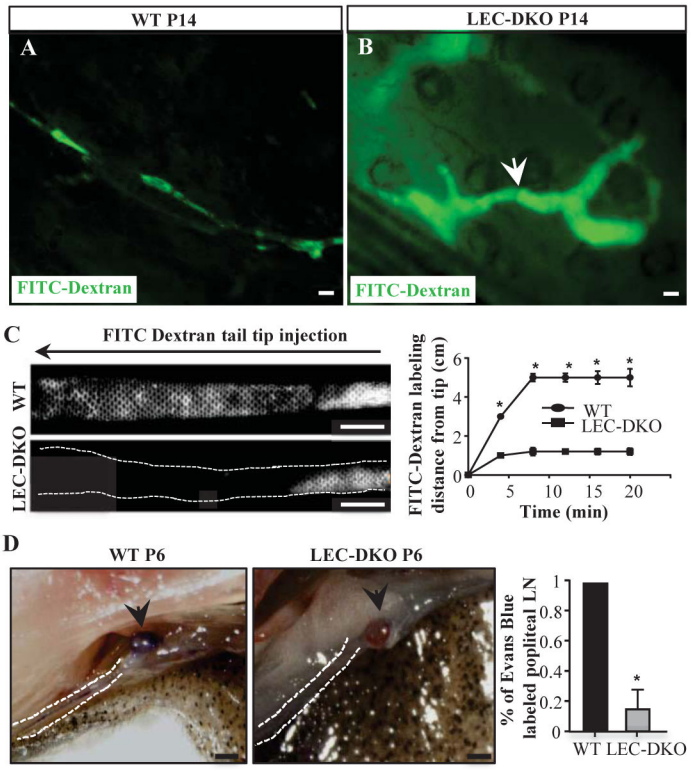

Fig. 2. Impaired lymphatic drainage in LEC-DKO mice

A–B) Representative images of ear lymphatic drainage after FITC-Dextran injection in P14 wild-type (A) and LEC-DKO (B) mice (n=9 mice per group). Arrow indicates a defective valve. Scale bar, 50 μm. **C)** Representative fluorescence microlymphangiography of FITC-Dextran injection into tail tips of P14 wild-type (n=4) and LEC-DKO mice (n=6) analyzed in 3 independent experiments. Black arrow above the images marks the direction of lymphatic transport. Scale bar, 1 cm. Quantification of FITC-Dextran labeling intensity is shown at right. Two-way ANOVA. **D)** Representative images of popliteal lymph nodes (black arrows) after Evans blue injection into hind foot pads of P6 wild-type and LEC-DKO pups (n=6 pups per group analyzed in 3 independent experiments). White dashed lines indicate a possible collecting lymphatic vessel. Scale bar, 5 mm. Quantification of Evans blue intensity is shown at right. All values are mean ± SD. *p<0.05; Logistic regression.

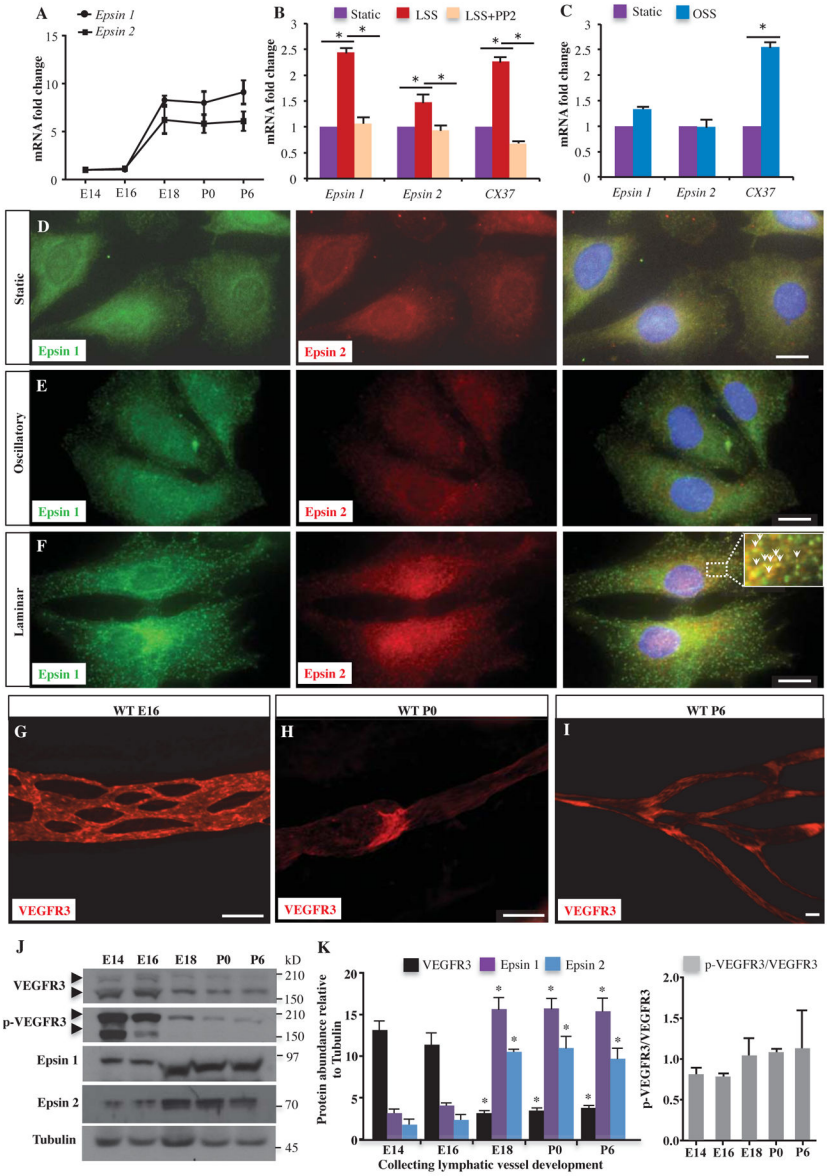

Fig. 3. Reciprocal expression of VEGFR3 and epsin in developing collecting lymphatic vessels

A) Quantification of qRT-PCR analysis of *epsin 1* and *epsin 2* mRNA in mesenteric lymphatics at developmental stages of E14, E16, E18, P0 and P6 (n=3 independent experiments). One-way ANOVA. **B)** Quantification of qRT-PCR analysis of *epsin 1*, *epsin 2* and *CX37* mRNA from mouse LECs pretreated with or without PP2 under steady shear stress or static conditions (n=3 independent experiments). One-way ANOVA. **C)** Quantification of qRT-PCR analysis of *epsin 1*, *epsin 2* and *CX37* mRNA from mouse LECs under laminar shear stress or static conditions (n=3 independent experiments). All values are mean ± SD. **p*<0.05; Student t test. **D–F)** Representative immunostaining of mouse LECs after 16 hours of static, laminar shear stress or oscillatory shear stress conditions using antibodies against epsin 1, epsin 2 and counterstained with DAPI (n=3 independent experiments). Scale bar, 10 μm. White arrow indicates the colocalization of epsin 1 and

epsin 2. **G–I**) Representative whole mount immunostaining of wild-type mesenteric collecting lymphatic vessels at developmental stages E16 (n=6 embryos) (G), P0 (n=5 pups) (H), and P6 (n=4 pups) (I) using antibodies against VEGFR3. Scale bar, 50 μm. **J)** Western blot analysis of epsin 1, epsin 2, VEGFR3, and p-VEGFR3 in isolated mesenteric LECs at developmental stages E14, E16, E18, P0 and P6. **K)** Quantification of epsin 1, epsin 2, and VEGFR3 protein abundance normalized to Tubulin (left panel) and VEGFR3 phosphorylation normalized to total VEGFR3 abundance (right panel) (n=3 independent experiments). All values are mean ± SD. *p<0.05 compared to E14; One-way ANOVA.

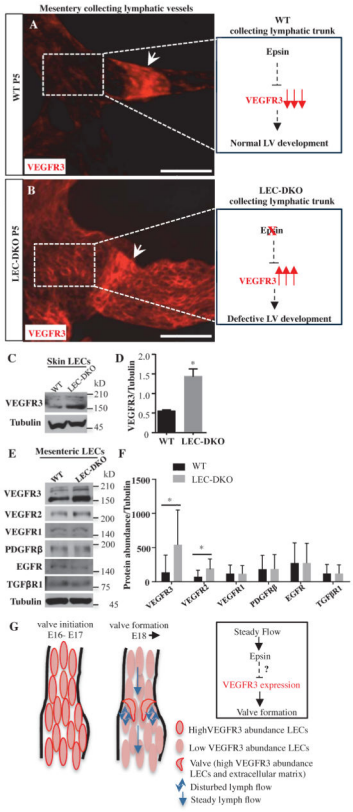

Fig. 4. Increased VEGFR3 abundance in LEC-DKO collecting lymphatic trunk LECs

A–B) Representative whole mount immunostaining of wild-type (A) and LEC-DKO (B) mesenteric collecting lymphatic vessels at P5 using antibodies against VEGFR3 (n=5 pups per group). White arrows indicate lymphatic valves. The diagrams at the right are models for how epsin 1 and 2 facilitate the decrease in VEGFR3 abundance in collecting lymphatic trunk LECs to ensure proper valve formation. Scale bar, 100 μm. **C)** Western blotting analysis of VEGFR3 abundance in skin LECs from WT and LEC-DKO mice. **D)** Quantification of VEGFR3 abundance normalized to Tubulin (n=3 independent experiments). **E)** Western blotting analysis of VEGFR3, VEGFR2, VEGFR1, EGFR, PDGFRβ, and TGFβR1 abundance in mesenteric LECs from WT and LEC-DKO mice. **F)** Quantification of receptor protein fold changes normalized to Tubulin (n=3 independent experiments). All values are mean ± SD. *p<0.05; One-way ANOVA. **G)** Schematic summary of the predicted roles of epsins in temporally and spatially regulating VEGFR3 abundance during lymphatic valve formation. Blue arrow indicates the two different types of lymph flow. Diagram at the right indicates the possible regulatory role of epsins which are increased by steady flow thus reducing VEGFR3 abundance to ensure proper valve formation.

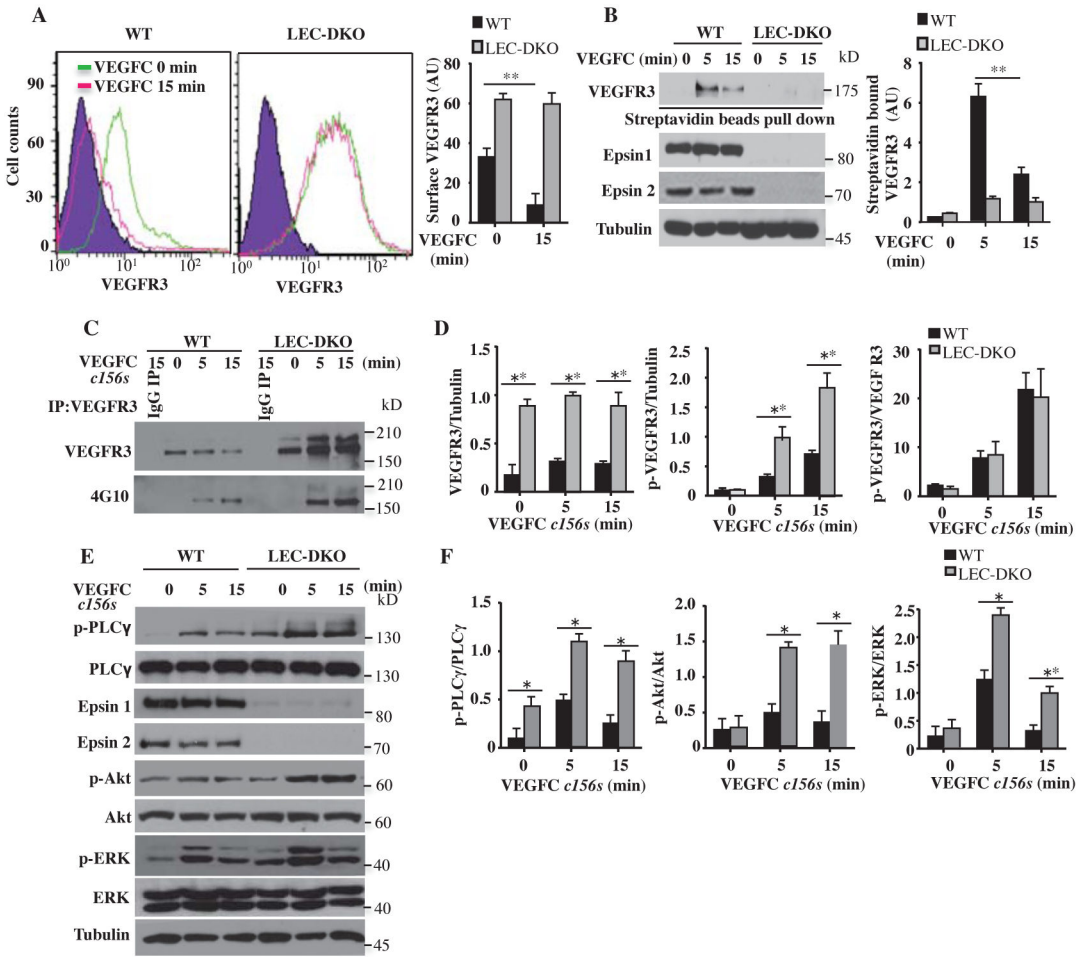

Fig. 5. Decreased ligand-induced VEGFR3 internalization and signaling termination in epsin-deficient LECs

A) FACS analysis of the surface abundance of VEGFR3 in LECs from wild-type or LEC-DKO mice. Quantification is shown at right (n=6 independent experiments). **B)** Western blot analysis of internalized biotinylated VEGFR3 detected by pull down with streptavidin beads and Western blotting with VEGFR3 antibodies. Quantification of VEGFR3 internalization is shown at right (n=4 independent experiments). **C)** Mouse LECs from wild-type and LEC-DKO mice were stimulated with VEGFC *c156s* for indicated time points and lysates were followed by immunoprecipitation with VEGFR3 antibodies or control IgG. Phospho-VEGFR3 signals were detected by Western blotting using 4G10 antibodies. **D)** Quantification of total and phosphorylated VEGFR3 shown in (C) (n=3 independent experiments). **E)** Mouse LECs from wild-type and LEC-DKO mice were stimulated with VEGFC *c156s* for the indicated time points, and VEGFR3 downstream signaling was analyzed by Western blotting with the indicated antibodies. **F)** Quantification of VEGFR3 downstream signaling shown in (E) (n=3 independent experiments). All values are mean ± SD. **p*<0.05; ***p*<0.01; Two-way ANOVA.

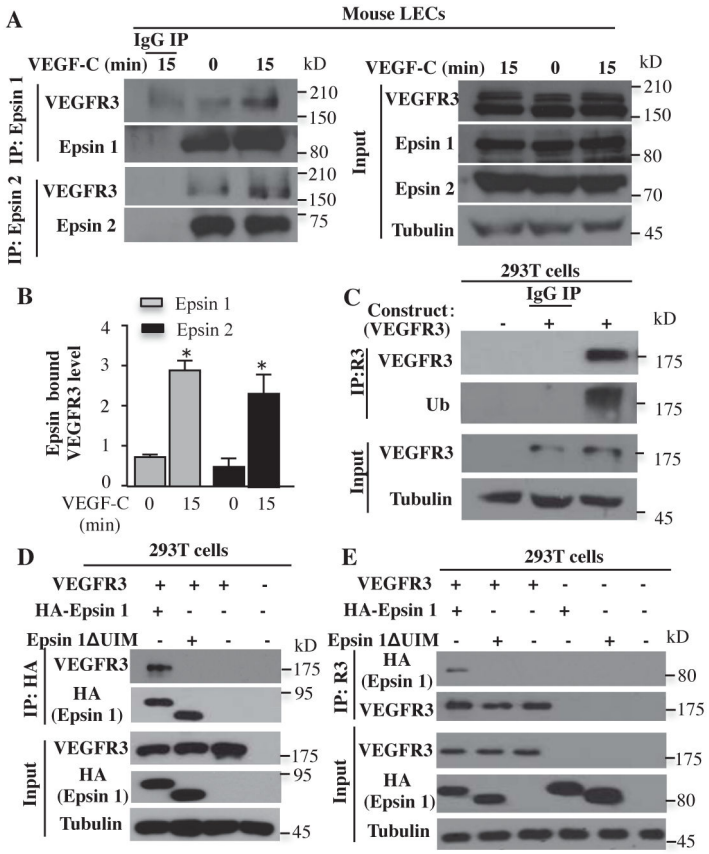

Fig. 6. Epsin interacted with activated VEGFR3 through its UIM domain

A) Mouse LECs were stimulated with VEGF-C for indicated time points and lysed followed by immunoprecipitation with epsin 1 antibodies or control IgG. Interactions were detected by Western blotting with the indicated antibodies. **B)** Quantification of epsin 1-bound VEGFR3 (n=3 independent experiments) and epsin 2-bound VEGFR3 (n=3 independent experiments). All values are mean ± SD. *$p<0.05$; One-way ANOVA. **C)** Lysates from HEK 293T cells expressing VEGFR3 or empty vector were stimulated with VEGF-C and then immunoprecipitated with VEGFR3 antibodies then Western blotted with ubiquitin antibodies (n=3 independent experiments). Ub: ubiquitin. **D)** Lysates from HEK 293T cells expressing combinations of VEGFR3, HA-epsin 1, HA-epsin 1ΔUIM, or empty vector and stimulated with VEGF-C for 15 minutes were immunoprecipitated with HA antibodies or control IgG and Western blotted with the indicated antibodies (n=3 independent experiments). **E)** Lysates from HEK 293T cells expressing combinations of VEGFR3, HA-epsin 1, HA-epsin 1ΔUIM, or empty vector and stimulated with VEGF-C were immunoprecipitated with VEGFR3 antibodies or control IgG and Western blotted with the indicated antibodies (n=3 independent experiments).

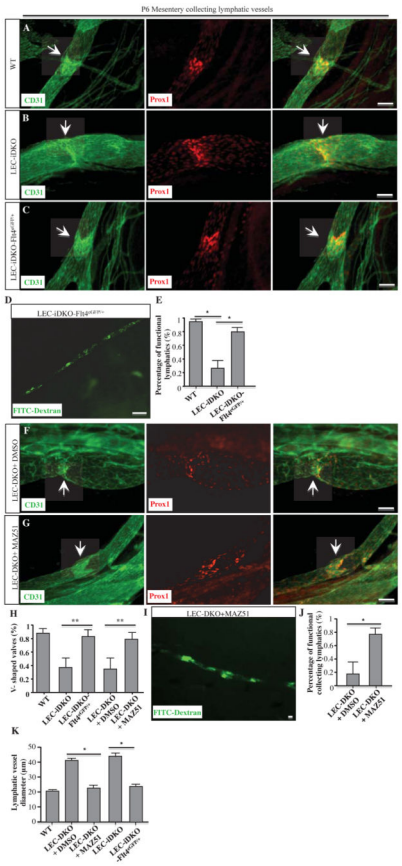

Fig. 7. Improved lymphatic valve formation by reducing VEGFR3 abundance or activity in epsin-deficient mice

A–C) Representative whole mount immunostaining of mesenteric lymphatic valves of P6 wild-type mice (A), LEC-iDKO mice (B), and LEC-iDKO-Flt4$^{eGFP/+}$ mice (C). White arrow indicates potential lymphatic valve region. Scale bar, 50 μm. **D)** Representative image of lymphatic drainage after FITC-Dextran injection into the footpads of P6 LEC-iDKO-Flt4$^{eGFP/+}$ mice. Scale bar, 50 μm. **E)** Quantification of percentage of functional collecting lymphatic vessels assessed as in (C) in P6 wild-type, LEC-iDKO or LEC-iDKO-Flt4$^{eGFP/+}$ pups (n=3 pups per group analyzed in 3 independent experiments). All values are mean ± SD. *p<0.05; Logistic regression. **F–G**) Representative whole mount immunostaining of mesenteric lymphatic valves of P6 LEC-DKO mice treated with DMSO (F) or LEC-DKO mice treated with MAZ51 (G). White arrow indicates potential lymphatic valve region. Scale bar, 50 μm. **H)** Quantification of percentage of V-shape mesenteric lymphatic valves in (A–C) and (F–G) (n=3 pups per group analyzed in 3 independent experiments). All values are mean ± SD. **p<0.01; Logistic regression. **I)** Representative image of lymphatic drainage after FITC-Dextran injection into footpads of P6 LEC-DKO mice treated with MAZ51. Scale bar, 50 μm. **J)** Quantification of percentage of functional collecting lymphatic vessels in P6 LEC-DKO pups assessed as in (I) after treatment with DMSO or MAZ51 (n=6 pups per group analyzed in 3 independent experiments). All values are mean ± SD. *p<0.05; Logistic regression. **K**) Quantification of mean lymphatic vessel diameters in P6 DMSO-treated LEC-DKO, MAZ51-treated LEC-DKO, LEC-iDKO, LEC-iDKO-

Flt4$^{eGFP/+}$ and wild-type intestinal capillary. Statistically significant differences are indicated. All values are mean ± SD (n=3 embryos per group analyzed in 3 independent experiments). *p<0.05; One-way ANOVA.